

NUMERICAL RENORMALIZATION GROUP ALGORITHMS FOR SELF-SIMILAR SOLUTIONS OF PARTIAL DIFFERENTIAL EQUATIONS

GASTÃO A. BRAGA, FREDERICO C. FURTADO, AND LONG LEE

ABSTRACT. We introduce and systematically investigate a numerical procedure that reveals the asymptotically self-similar dynamics of solutions of partial differential equations (PDEs). The approach is based on the renormalization group (RG) theory for PDEs. This numerical version of RG method, dubbed as the numerical RG algorithm, numerically rescales the temporal and spatial variables in each iteration and drives the solutions to a fixed point exponentially fast, which corresponds to self-similar dynamics of the equations. Moreover, the procedure allows us for detecting and further finding the critical exponent of the logarithmic decay hidden in self-similar solutions. We carefully examine the ability of the algorithm for determining the critical scaling exponents in time and space that render explicitly the distinct physical effects of the solutions of the Burgers equation, depending on the initial conditions. We use the phenomena of dispersive shock waves of the Korteweg-de Vries equation to show that the algorithm can be used as a time integrator for investigating intermediate asymptotic behavior of solutions. Finally, we illustrate the ability of the numerical RG procedure for detecting and capturing the hidden logarithmic decay through a nonlinear system of cubic autocatalytic chemical reaction equations.

keywords: Self-similar dynamics, renormalization group transformation, asymptotic limit, critical exponent, Burgers equation, dispersive shock wave, Korteweg-de Vries (KdV) equation, intermediate asymptotic behavior, nonlinear chemical reaction.

1. INTRODUCTION

Solutions of certain partial differential equations (PDEs) exhibit self-similar dynamics in the asymptotic limit. A self-similar solution in the region of large-time asymptotic limit normally is in the form of

$$u(x, t) \sim \frac{A}{t^\alpha} \phi\left(B \frac{x}{t^\beta}\right), \quad \text{as } t \rightarrow \infty. \quad (1)$$

This particular form of solution indicates that in the large-time asymptotic region the dynamics of the solution are controlled by two factors, the decay in the magnitude of u and the spread of the spatial distribution of u , while the profile of the self-similar solution is described by the function ϕ . The constant A and B in Eq. (1) are usually related to some conservation laws of the PDE under study. In the literature, physicists were able to predict or determine the scaling exponents α and β for critical phenomena by using the renormalization group (RG) approach for a variety of physical models in equilibrium statistical mechanics or quantum field theory. [19, 20, 29, 33, 34]. In the early 1990s, Goldenfeld et al. developed a perturbative renormalization group method for PDEs and applied it to the study of a number of large-time asymptotic problems [15, 20–22]. A slight twist of the original method was reported in [13, 14, 26]. Almost at the same period, a nonperturbative RG approach was introduced by Bricmont et al. [10, 12], and was applied to the study of nonlinear dispersive and dissipative wave equations and thermal-diffusive combustion system [7, 11, 27].

Also in the 1990s, Chen and Goldenfeld proposed a numerical RG calculation for similarity solutions of porous medium (Barenblatt) equation and traveling waves [16]. Their numerical procedure inspired mesh renormalization schemes for studying focusing problems arising in porous medium flow [4, 6]. In this paper, combining the numerical approach of Chen and

Goldenfeld with the nonperturbative RG approach of Bricmont et al., we introduce a numerical RG algorithm that allows us systematically search for the critical exponents and the hidden decay in asymptotically self-similar dynamics through repeated scalings in time and space. We note that a numerical RG procedure with the similar sprit as the proposed algorithms was introduced by Braga et al. [9] for studying a nonlinear diffusion equation with periodic coefficients.

Numerical procedures based on rescaling have previously been developed and used to study solutions which blow up in finite time [5, 18, 24, 28]. Such procedures exploit the known self-similar structure of the solutions under study to determine the appropriate rescalings. The proposed RG algorithm in this paper, however, is unique in exploiting fixed points by generating successive iterations of a discrete RG transformation in space and time that drive the system towards a fixed point, and the current implementation of the proposed algorithm is not suitable for studying blow-up problems.

Finally, we remark that the focus of this paper is to introduce a numerical algorithm and to demonstrate the effectiveness and robustness of the algorithm. The self-similar dynamics of the PDEs illustrated in the following examples are all well-studied theoretically. The application of the proposed algorithm to the solutions of certain physical models whose asymptotic self-similar dynamics are difficult to be obtained analytically is currently under our investigation and will be reported in a separate paper.

2. SCALING TRANSFORMATION FOR BURGERS EQUATION

The numerical RG method for PDEs is simply the integration of the equations over a finite time-interval with fixed length followed by a rescaling. To explain this idea, we use the Burgers equation as an example to illustrate the scaling transformation procedure of numerical RG algorithms. We compare the asymptotic solutions obtained by the numerical RG algorithm with the exact solutions in the asymptotic region to demonstrate the robust nature of our algorithm.

The Burgers equation with initial data at $t = 1$ are written as

$$\begin{aligned} u_t + uu_x &= \nu u_{xx}, \quad t > 1, \\ \text{I. C. : } u(x, 1) &= f(x), \end{aligned} \quad (2)$$

where $\nu > 0$ is the viscosity. Let the time and space variables be scaled by powers of a fixed length $L > 1$,

$$t = L\tilde{t}, \quad x = L^\beta \tilde{x}, \quad (3)$$

where $\beta > 0$, \tilde{t} and \tilde{x} are new variables. Suppose the solution of the initial value problem (IVP) (2), $u(x, t)$, is scaled by

$$u_L(\tilde{x}, \tilde{t}) = L^\alpha u(x, t) = L^\alpha u(L^\beta \tilde{x}, L\tilde{t}), \quad (4)$$

where $\alpha > 0$. This implies that

$$u(x, t) = L^{-\alpha} u_L(\tilde{x}, \tilde{t}) = L^{-\alpha} u_L(L^{-\beta} x, L^{-1} t). \quad (5)$$

With the above scalings, each term in the Burgers equation is scaled as follows:

$$u_t = L^{-(\alpha+1)} \frac{\partial}{\partial \tilde{t}} (u_L(\tilde{x}, \tilde{t})), \quad u_x = L^{-(\alpha+\beta)} \frac{\partial}{\partial \tilde{x}} (u_L(\tilde{x}, \tilde{t})), \quad u_{xx} = L^{-(\alpha+2\beta)} \frac{\partial^2}{\partial \tilde{x}^2} (u_L(\tilde{x}, \tilde{t})). \quad (6)$$

Substituting Eq. (6) into Eq. (2) yields

$$\begin{aligned} L^{-(\alpha+1)} (u_L)_{\tilde{t}} + L^{-(2\alpha+\beta)} u_L (u_L)_{\tilde{x}} &= \nu L^{-(\alpha+2\beta)} (u_L)_{\tilde{x}\tilde{x}}, \quad \tilde{t} > 1, \\ \text{I. C. : } u_L(\tilde{x}, 1) &= \tilde{f}(\tilde{x}), \end{aligned} \quad (7)$$

We rewrite the above equation as

$$(u_L)_{\tilde{t}} + L^{-\alpha-\beta+1}u_L(u_L)_{\tilde{x}} = \nu L^{-2\beta+1}(u_L)_{\tilde{x}\tilde{x}}, \quad \tilde{t} > 1, \quad (8)$$

$$\text{I. C. : } u_L(\tilde{x}, 1) = \tilde{f}(\tilde{x}).$$

The integration length for time is from $t = 1$ to $t = L$, while the transformed initial condition is $\tilde{f}(\tilde{x}) = L^\alpha u(L^\beta \tilde{x}, L)$.

2.1. Sequence of Scaling Transformations. If we perform a sequence of scalings (iterations), then with a fixed $L > 1$, and sequences of scaling exponents $\{\alpha_n\}$ and $\{\beta_n\}$, we can define a sequence of rescaled functions $\{u_n\}$ by rewriting Eq. (4) (dropping $\tilde{\cdot}$ in \tilde{x} and \tilde{t}) as

$$u_n(x, t) = L^{\alpha_n} u_{n-1}(L^{\beta_n} x, Lt), \quad (9)$$

with $u_0 = u$ of the original IVP, Eq. (2). A simple calculation reveals that

$$\begin{aligned} u_n(x, t) &= L^{(\alpha_1+\alpha_2+\alpha_3+\dots+\alpha_n)} u(L^{(\beta_1+\beta_2+\beta_3+\dots+\beta_n)} x, L^n t) \\ &= L^{n\bar{\alpha}_n} u(L^{n\bar{\beta}_n} x, L^n t), \end{aligned} \quad (10)$$

where $\bar{\alpha}_n = \frac{1}{n}(\alpha_1 + \alpha_2 + \dots + \alpha_n)$ and $\bar{\beta}_n = \frac{1}{n}(\beta_1 + \beta_2 + \dots + \beta_n)$. Eq. (10) shows how u_n in the time interval $t \in [1, L]$ is related to u in the time interval in $t \in [L^n, L^{n+1}]$. Since at each iteration, the scaling of the PDE shown in Eq.(8) is applied to the previous scaled equation, the solution of the n^{th} iteration, $u_n(x, t)$, is the solution of the following scaled initial value problem

$$(u_n)_t + L^{n(-\bar{\alpha}_n-\bar{\beta}_n+1)}u_n(u_n)_x = \nu L^{n(-2\bar{\beta}_n+1)}(u_n)_{xx}, \quad t > 1, \quad (11)$$

$$\text{I. C. : } u_n(x, 1) = f_n(x),$$

where $f_n(x) = L^{\alpha_n} u_{n-1}(L^{\beta_n} x, L)$, with $f_0 = f$, the initial condition of the IVP (2).

A simple observation for the scaled IVP (11) is that if $\bar{\alpha}_n \rightarrow 1/2$ and $\bar{\beta}_n \rightarrow 1/2$ as $n \rightarrow \infty$, the diffusion term has unscaled viscosity and the pre-factor of the quasilinear term in the left-hand-side is of order 1 for sufficiently large n . In this case, for small viscosity, the long-time behavior of the solution is dominated by the quasilinear term. On the other hand, if $\bar{\alpha}_n \rightarrow 1$ and $\bar{\beta}_n \rightarrow 1/2$ as $n \rightarrow \infty$, the viscosity in the diffusion term remains unscaled, but the advection term on the left-hand-side has L to the power of negative $n/2$. With $L > 1$ and $n \rightarrow \infty$, the advection term eventually drops out the equation, and the diffusion will be the dominant term. The numerical renormalization group calculations based on the algorithm in the next section confirm that for positive mass initial data, it is the former case, while for the zero mass initial data, it is the later one. There is a third possibility, $\bar{\alpha}_n \rightarrow 0$ and $\bar{\beta}_n \rightarrow 1$ as $n \rightarrow \infty$, corresponding to the traveling wave solutions of the Burgers equation, that we do not discuss in this paper.

2.2. Numerical RG procedure. We describe the numerical RG procedure in Algorithm 1. Note that in Step 4. of Algorithm 1, the variable A_n is defined, as now we explain, based on the assumption that for the solution of Eq. (2), denoted $u(x, t)$, there exists a self-similar profile function ϕ such that

$$u(x, t) \sim \frac{A}{t^\alpha} \phi\left(B \frac{x}{t^\beta}\right), \quad \text{as } t \rightarrow \infty, \quad (12)$$

where A is some constant and α and β are the powers of decay and spreading with respect to time, respectively. After n iterations, $t = L^n$, and hence Eq. (12) becomes

$$u(x, L^n) \sim \frac{A}{L^{n\alpha}} \phi\left(B \frac{x}{L^{n\beta}}\right), \quad (13)$$

Algorithm 1 Numerical RG procedure for the Burgers equation

for $n = 0, 1, 2, \dots$, until convergence **do**

1. Start with the IVP (2) for $n = 0$. Evolve u_n from $t = 1$ to $t = L$, using the IVP (11) for $n \geq 1$.
2. Compute α_{n+1} by

$$L^{\alpha_{n+1}} = \frac{\|u_n(\cdot, 1)\|_\infty}{\|u_n(\cdot, L)\|_\infty} = \frac{\|u(L^n \bar{\beta}_n, L^n)\|_\infty}{\|u(L^n \bar{\beta}_n, L^{n+1})\|_\infty}.$$

3. Compute β_{n+1} from an appropriate scaling relation between α_{n+1} and β_{n+1} . Normally, $\beta_{n+1} = g(\alpha_{n+1})$, for some function g .
4. Compute $A_n = L^{n(\alpha_n - \bar{\alpha}_n)}$, $B_n = L^{n(\beta_n - \bar{\beta}_n)}$, and $f_{n+1}(x) = L^{\alpha_{n+1}} u_n(L^{\beta_n} x, L)$, where $\bar{\alpha}_n = \frac{1}{n}(\alpha_1 + \alpha_2 + \dots + \alpha_n)$ and $\bar{\beta}_n = \frac{1}{n}(\beta_1 + \beta_2 + \dots + \beta_n)$.

end for

which implies that for large n

$$L^{n\alpha} u(L^{n\beta} x, L^n) \sim A\phi(Bx). \quad (14)$$

Suppose that $\alpha_n \rightarrow \alpha$ and $\beta_n \rightarrow \beta$, as $n \rightarrow \infty$, Eq. (14) is equivalent to

$$L^{n\alpha} u(L^{n\beta} x, L^n) \sim A\phi(Bx), \quad n \rightarrow \infty. \quad (15)$$

From Eq. (10), we have

$$L^{-n\bar{\alpha}_n} u_n(L^{-n\bar{\beta}_n} x, t) = u(x, L^n t). \quad (16)$$

Letting $t = 1$ in Eq. (16), Eqs. (15) and (16) together imply that

$$L^{n(\alpha_n - \bar{\alpha}_n)} u_n(L^{n(\beta_n - \bar{\beta}_n)} x, 1) \sim A\phi(Bx). \quad (17)$$

If we define $A_n = L^{n(\alpha_n - \bar{\alpha}_n)}$, $B_n = L^{n(\beta_n - \bar{\beta}_n)}$, we expect that

$$\lim_{n \rightarrow \infty} A_n = \lim_{n \rightarrow \infty} L^{n(\alpha_n - \bar{\alpha}_n)} \rightarrow A, \quad \lim_{n \rightarrow \infty} B_n = \lim_{n \rightarrow \infty} L^{n(\beta_n - \bar{\beta}_n)} \rightarrow B, \quad (18)$$

provided

$$u_n(L^{n(\beta_n - \bar{\beta}_n)} x, 1) \rightarrow \phi(Bx). \quad (19)$$

2.3. Numerical experiments. We now describe the simple explicit algorithm used for solving the scaled PDE (11). Suppose that within each iteration of the numerical RG algorithm, we discretize the spatial derivatives by the centered difference scheme and use the first-order Euler method for our temporal discretization. If we denote

$$\kappa_n = L^{n(-\bar{\alpha}_n - \bar{\beta}_n + 1)}, \quad \nu_n = \nu L^{n(-2\bar{\beta}_n + 1)}, \quad v = u_n, \quad (20)$$

at time $t^{j+1} = (j+1)\Delta t$, the fully discretized scaled equation of Eq. (11) at the i^{th} grid point is

$$v_i^{j+1} = v_i^j - \Delta t \frac{\kappa_n}{2} \left(\frac{(v_{i+1}^j)^2 - (v_{i-1}^j)^2}{2\Delta x_n} \right) + \Delta t \nu_n \left(\frac{v_{i-1}^j - 2v_i^j + v_{i+1}^j}{\Delta x_n^2} \right), \quad (21)$$

where Δx_n is the spatial grid size for the n^{th} iteration. From Eq. (9), suppose that we denote the i^{th} spatial node on a uniform mesh at the n^{th} iteration as $(x_i)_n = i\Delta x_n$, where $i = 0, \pm 1, \pm 2, \dots$, we have

$$u_n(i\Delta x_n, t) = L^{\alpha_n} u_{n-1}(L^{\beta_n} i\Delta x_n, Lt) = L^{\alpha_n} u_{n-1}(i\Delta x_{n-1}, Lt). \quad (22)$$

This implies that

$$\Delta x_n = L^{-\beta_n} \Delta x_{n-1}. \quad (23)$$

Since $L > 1$, if $\beta_n > 0$ for all n then $\Delta x_n < \Delta x_{n-1} < \Delta x_{n-2} < \dots < \Delta x_0$, and for sufficiently large n , $\Delta x_n \ll \Delta x_0$. If a uniform Δt is used for all iterations, this could lead to numerical instability at later iterations for an explicit time integrator, such as the Euler method adopted in this paper. Conversely, if Δt decreases accordingly to maintain the stability requirement, eventually the time integration becomes too costly for the numerical RG algorithm. A remedy for this situation is that instead of scaling the mesh size, we keep the same Δx at all time, i.e. $\Delta x_n = \Delta x_{n-1} = \dots = \Delta x_0 = \Delta x$, through interpolation. To explain this idea, we see that at the end of the first iteration ($n = 0$), we are supposed to set the initial data at the j^{th} node for the next iteration to be $f_1(x_j) = f_1(L^{\beta_1} j \Delta x_1) = L^{\alpha_1} u_0(j \Delta x_0, L)$, or equivalently $f_1(x_j) = f_1(j \Delta x_1) = L^{\alpha_1} u_0(L^{-\beta_1} j \Delta x_0, L)$. If we choose x_j on the new grid to be the same as that of the old grid, i.e. $j \Delta x_1 = j \Delta x_0$, we need the value $u_0(L^{-\beta_1} j \Delta x_0, L)$. Since $u_0(j \Delta x_0, L)$ has been computed for each j , to obtain $u_0(L^{-\beta_1} j \Delta x_0, L)$, we can simply linearly interpolate $u_0(k \Delta x_0, L)$ and $u_0((k+1) \Delta x_0, L)$, where $k \Delta x_0 < L^{-\beta_1} j \Delta x_0 < (k+1) \Delta x_0$ for some k . By repeating this process, we have $\Delta x = \Delta x_0 = \Delta x_1 = \Delta x_2 = \dots = \Delta x_n$. This strategy was first adopted by Chen and Goldenfeld [16].

2.3.1. *Positive initial mass.* The first initial condition we consider for our numerical experiments is the characteristic function

$$u(x, 0) = \chi_{[-\ell, \ell]}(x) = \begin{cases} 1, & -\ell \leq x \leq \ell, \\ 0, & \text{else.} \end{cases} \quad (24)$$

It is known that a conserved quantity of the Burgers equation is the total mass defined by

$$M = \int_{-\infty}^{\infty} u(x, t) dx. \quad (25)$$

For the characteristic function, the total mass is trivial to compute initially.

Whitham [32] showed that a special asymptotic self-similar solution of single hump for the Burgers equation with initial data possessing positive total mass has the following explicit formula (page 104, Eq. (4.32)):

$$u(x, t) = \sqrt{\frac{2M}{t}} g(z, R), \quad (26)$$

where $M > 0$ is the total mass of initial data, $z = x/\sqrt{2Mt}$ is the similarity variable, and $R = M/(2\nu)$ is the Reynolds number, where ν is the viscosity. The function $g(z, R)$ is

$$g(z, R) = \frac{(e^R - 1)}{2\sqrt{R}} \frac{e^{-z^2 R}}{\sqrt{\pi} + (e^R - 1) \int_{z\sqrt{R}}^{\infty} e^{-\xi^2} d\xi}. \quad (27)$$

Based on dimensional arguments, Whitham indicated that the similarity form of the above solution is

$$u(x, t) = \sqrt{\frac{\nu}{t}} \phi\left(\frac{x}{\sqrt{\nu t}}; \frac{M}{\nu}\right). \quad (28)$$

Comparing Eq. (12) and Eq. (28), we expect that the sequences of exponents $\{\alpha_n\}$ and $\{\beta_n\}$ in the numerical RG converge to $\alpha = 1/2$ and $\beta = 1/2$, respectively, for sufficiently large iteration numbers. Hence our numerical RG procedure starts with letting $\beta_n = 1/2$ for all n . This means that the spatial variable is always scaled by $L^{-1/2}$ for the next iteration. As we mentioned earlier, this assumption also corresponds to ensuring that the viscosity remains the same at all time, that is $\nu_n = \nu$.

Comparing Eqs. (10) and (26), we see that the term $\sqrt{t} u(\hat{z}, t)$ is equivalent to $L^{n\bar{\alpha}_n} u(\hat{z}, L^n)$, where $\hat{z} = \sqrt{2M}z = \frac{1}{\sqrt{t}}x = L^{-n/2}x$ with $t = L^n$. With the assumption $\beta_n = 1/2$ for all n , we

have $\bar{\beta}_n = 1/2$, and $L^{-n\bar{\beta}_n} = \frac{1}{\sqrt{t}}$. Moreover, if $\{\alpha_n\}$ approaches to $1/2$ (later we will show in our numerical experiments that this is in fact the case), then $\bar{\alpha}_n \approx 1/2$ for sufficiently large n . Hence $L^{n\bar{\alpha}_n} \approx \sqrt{t}$. This implies

$$u_n(L^{-n/2}x, L^n) = L^{n/2}u(x, t) = \sqrt{t}u(x, t) = \sqrt{2M}g(z, R). \quad (29)$$

Now plugging $z = \frac{\hat{z}}{\sqrt{2M}}$ into $g(z, R)$ to obtain $g(\hat{z}, R)$, we have

$$u_n(L^{-n/2}x, L^n) = \sqrt{2M}g(\hat{z}, R). \quad (30)$$

Using Eq. (30), if we plot the normalized function of $\sqrt{2M}g(\hat{z}, R)$ versus \hat{z} (so that the amplitude is one), this should be equivalent to plotting u_n against $L^{-n/2}x$ at the time evolution $t = L^n$. We are now ready to compare the theoretical similarity profile derived by Whitham [32] (page 106, Figure 4.1) and the one obtained from our numerical RG procedure. Figure 1 is the comparison of numerical RG calculations and the theoretical asymptotic solutions. For each case (a), (b), and (c) of Figure 1, the initial mass is $M = 1, 1,$ and 2 , respectively ($\ell = 1/2, 1/2$ and 1 , respectively in Eq. (24)), while the diffusivity constant is $\nu = 0.01, 0.05,$ and 0.01 , respectively. The figure shows that the numerical RG calculations remarkably capture the theoretical predictions for various initial data and diffusivity constant. In particular, the left panel plots the final waveform of the solution between the predicted theoretical profiles and that of our RG calculations, while the right panel indicates the convergence of A_n to its theoretical value A . Note that, integrating Eq. (17), and using Eqs. (18) and (19), the theoretical value A is given by

$$A = \frac{M}{\int_{\mathbb{R}} \phi(x) dx}, \quad (31)$$

where $\phi(x)$ is the computed RG profile. The total number of iterations for all three cases is $n = 500$. Within each iteration, the calculation was carried out in a periodic domain, $-8 \leq x \leq 8$, with $\Delta x = 16/5000$, while the time integration is from $t = 1$ to $t = L = 1.2$ with $\Delta t = 0.2/2000$. Figure 2 shows the calculations of α_n and κ_n . The figure indicates that $\alpha_n \rightarrow \frac{1}{2}$ and $\kappa_n \neq 0$ and is of $O(1)$. This suggests that in the asymptotical region the diffusion constant is unscaled. Since the diffusion constant is small and the coefficient of the advection is of order one in all three cases, the equation is advection dominant in the asymptotical region.

2.3.2. Zero initial mass. In this example, we consider the following initial condition for the Burgers equation

$$u_0(x) = -\chi_{[-\ell, 0]} + \chi_{[\ell, 0]} = \begin{cases} -1, & -\ell \leq x \leq 0, \\ 1, & 0 < x \leq \ell, \\ 0, & \text{else.} \end{cases} \quad (32)$$

The total mass of the above function is zero. For this initial condition, Whitham showed that for small diffusivity constants, the inviscid theory is adequate to explain the solutions of the Burgers equation for most of the range, except in the final decay period. The solutions are of typical N wave structures before the final decay. However, as $t \rightarrow \infty$, in the final decay, for any fixed diffusivity constant, no matter how small, the solution of the Burgers equation is

$$u(x, t) \sim \frac{x}{t} \sqrt{\frac{a}{t}} e^{-x^2/(4\nu t)}, \quad (33)$$

for some fixed a . Eq. (33) is the dipole solution of the heat equation, which means that the diffusion dominates the nonlinear term in the final decay, regardless the magnitude of the diffusivity constant. To study the final decay of solution by the numerical RG algorithm for this class of initial data, we let β in the spacial scaling be fixed and equal to $1/2$. This ensures that the coefficient in front of the diffusion term remains unscaled at all time. We set the

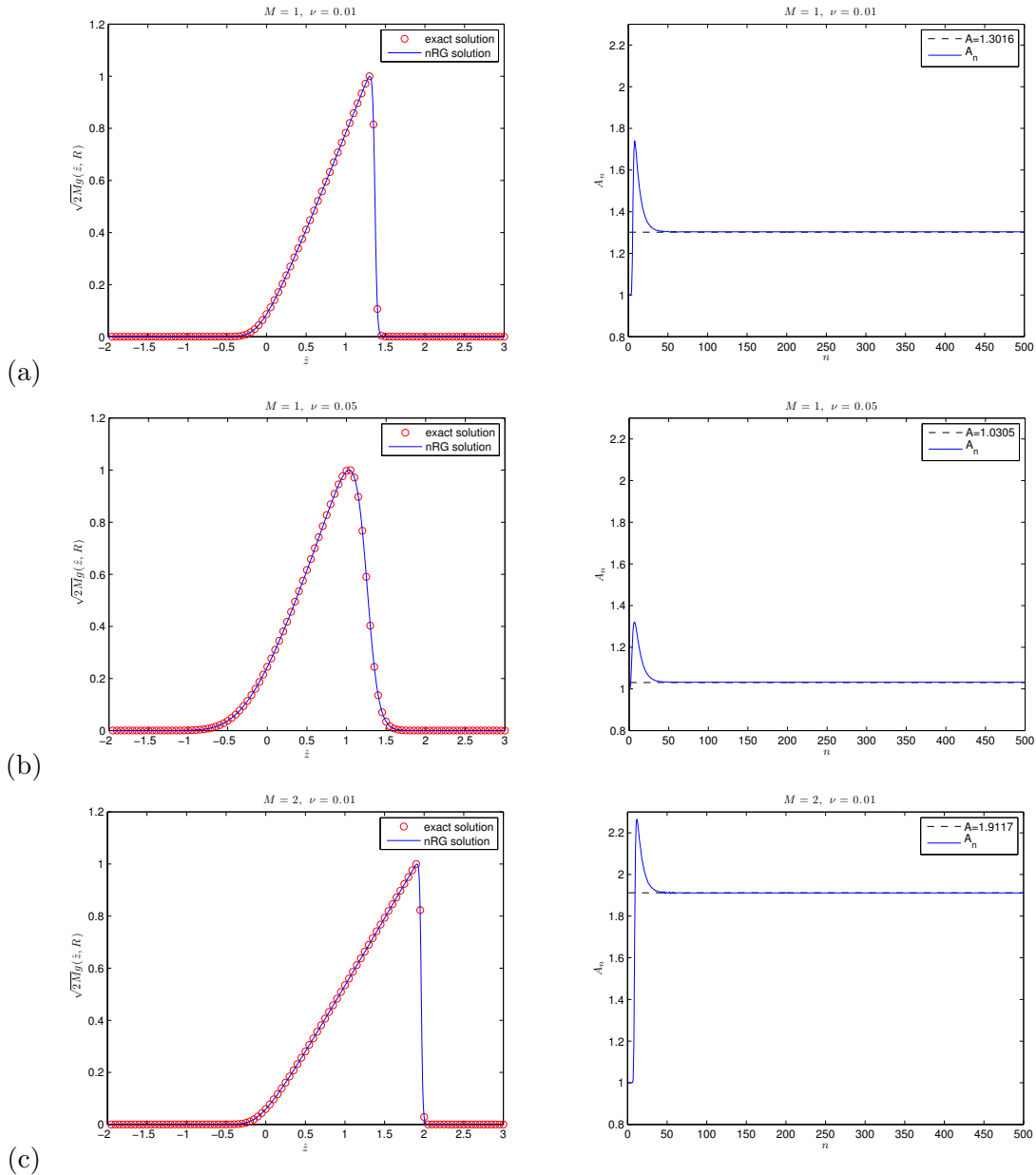


FIGURE 1. Comparisons between the numerical RG calculations and the asymptotic self-similar solutions shown in [32]. The left panel shows the waveforms of the RG solutions at the final iteration $n = 500$ and the theoretic predictions for various M and ν , while the right panel shows the convergence of A_n to its theoretical value A . The initial mass and viscosity used for the comparisons are (a) $M = 1$, $\nu = 0.01$, (b) $M = 1$, $\nu = 0.05$, and (c) $M = 2$, $\nu = 0.01$. All numerical calculations use $\Delta x = 0.0032$ and $\Delta t = 0.00001$.

diffusivity constant $\nu = 0.01$ and the parameter $L = 1.2$. The total number of iteration is $n = 1500$, and $\ell = 1$ in the initial condition. Figure 3(a) shows the snap shot of the numerical RG solution at the 400th iteration. It clearly shows that the solution is of the N wave structure at this stage. In Figure 3(b), the final profile of the numerical RG calculation at $n = 1500$ is compared with the dipole solution of heat equation. The fixed number a in Eq. (33) is

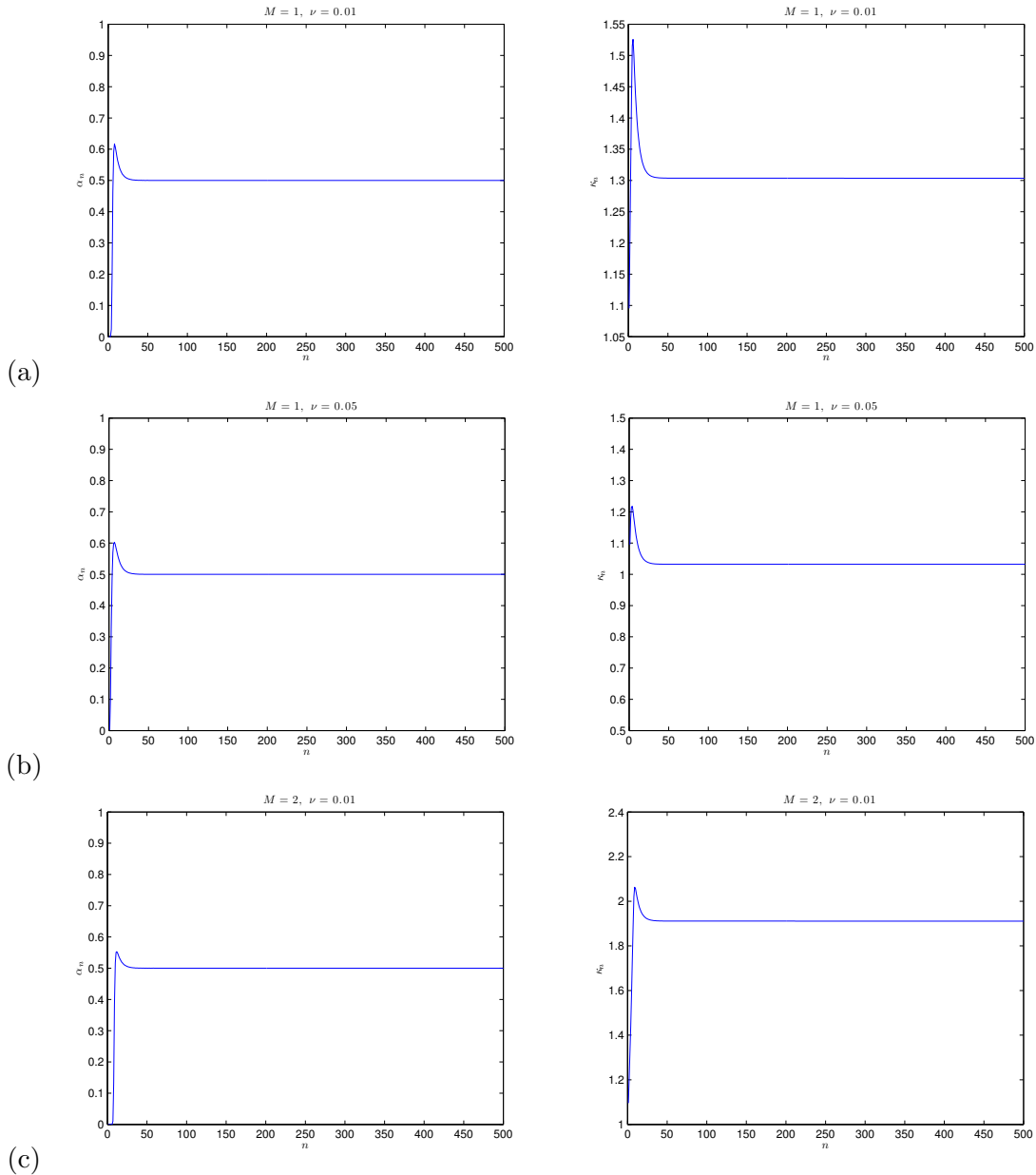


FIGURE 2. α_n (left) and κ_n (right) versus n (number of iteration). The initial mass and viscosity are the same as that in Figure 1 (a), (b), and (c). The figure indicates that $\alpha_n \rightarrow \frac{1}{2}$ and $\kappa_n \neq 0$ and is of $O(1)$, as expected.

chosen to be L^{2n} . Recall that the scaled spatial variable in the numerical RG calculation is $\hat{z} = L^{-n(1/2)}x = x/\sqrt{t}$. Substituting $a = L^{2n}$ and $\hat{z} = L^{-n(1/2)}x = x/\sqrt{t}$ into Eq. (33) and knowing that $L^{2n} = t^2$ yields the dipole solution as a function of the similarity variable \hat{z}

$$u(\hat{z}) = \hat{z}e^{-\hat{z}^2/(4\nu)}. \quad (34)$$

The circles in Figure 3(b) are the above dipole solution, with the amplitude being normalized to one, plotted against the similarity variable. The result of the numerical RG calculation at $n = 1500$ (the solid line in Figure 3(b)) correctly predicts the final decay. The convergences of the scaling parameters α_n and κ_n are shown in Figure 4(a) and (b), respectively. They indicate

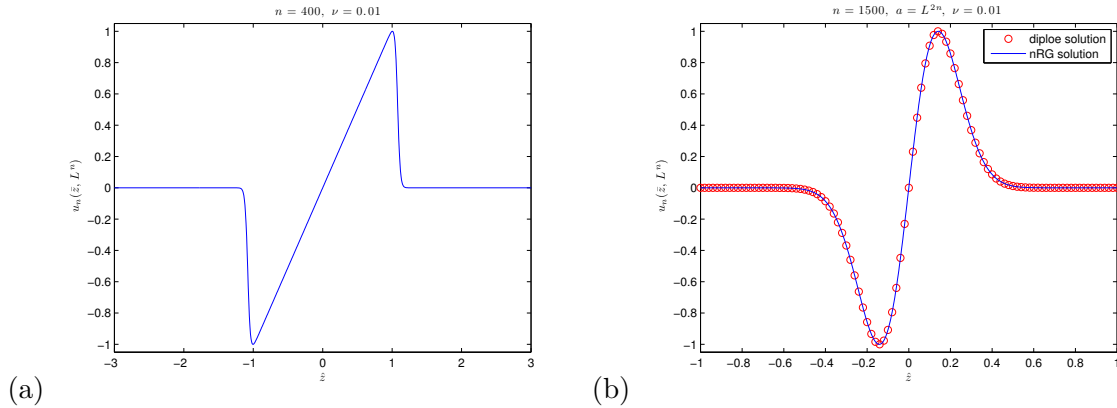


FIGURE 3. Numerical experiment with zero initial mass ($M = 0$). The viscosity is 0.01 ($\nu = 0.01$). (a) Waveform exhibiting N -wave structure computed by numerical RG at the 400th iteration. (b) Comparison between the asymptotic dipole-like solution and the numerical RG calculation at the 1500th iteration.

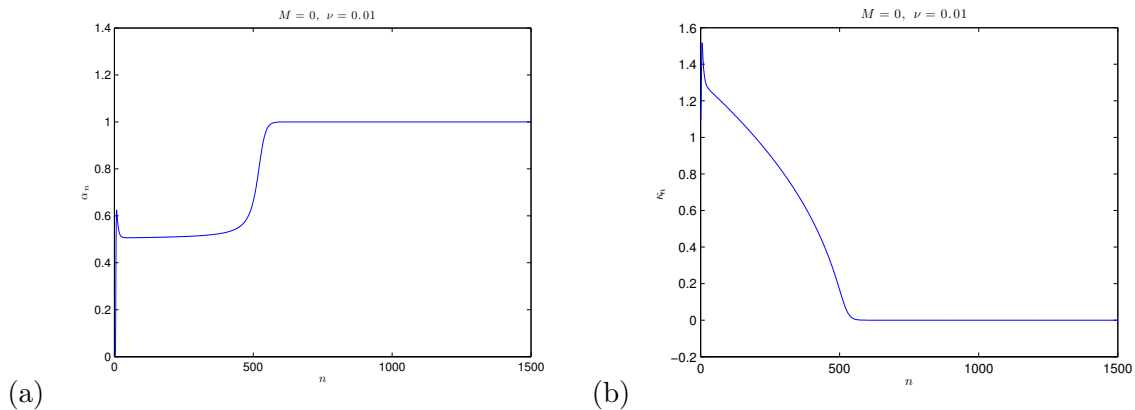


FIGURE 4. Scaled coefficients in the previous calculation (Figure 3). (a) α_n and (b) κ_n versus n (number of iteration).

that $\alpha_n \rightarrow 1$, which results in $\kappa_n \rightarrow 0$, where κ_n is the coefficient in front of the advection term of the scaled PDE. Such a convergence of κ_n suggests that the diffusion term dominates the final decay, regardless the magnitude of the diffusion constant, which is kept unscaled through out the calculation. These figures show the mechanism of the solution transiting from the N -wave structure to the dipole solution, as predicted in Whitham's analysis. The choice of the periodic domain, Δx , and Δt is the same as that used in Figure 1.

We remark that to prevent the numerical artifacts from distorting the symmetry of the solution during the step of normalizing the amplitude, we apply the negative mirror image of the right hump for the left one at the end of each time evolution.

3. KORTEWEG-DE VRIES EQUATION AND DISPERSIVE SHOCK WAVES

In this section, we illustrate that numerical RG procedure is an efficient method for studying asymptotic behavior of dispersive shock waves (DSWs). DSWs appear when dispersion dominates dissipation for step-like data; they have been seen in plasmas, fluids, superfluids and optics [2]. In a sequence of papers, Ablowitz et al. analyze interactions and asymptotics of DSWs for the Korteweg-de Vries (KdV) equation [1–3]. KdV equation is chosen for their

study because it is the leading-order asymptotic equation for weakly dispersive and weakly non-linear systems.

Consider the dimensionless form of KdV equation

$$u_t + uu_x + \epsilon^2 u_{xxx} = 0, \quad (35)$$

with $u = u(x, t)$ going rapidly to the boundary conditions

$$\lim_{x \rightarrow -\infty} u(x, t) = 0, \quad \lim_{x \rightarrow \infty} u(x, t) = -6c^2. \quad (36)$$

Single stepwise initial data for the above problem evolves to a wedge-shape envelope combining three basic regions: exponential decay region on the right, the DSW region in the middle, and the region of oscillating tail on the left [2]. All three regions travel to the left with time at a speed $x = -12c^2t$, while the DSW region is expanding and is of the order $O(t)$ [2, 3]. The amplitude of the DSWs saturates at $6c^2$.

The KdV equation for the described problem can be posed as an initial-boundary-value problem (IBVP) on a truncated domain $-\ell \leq x \leq \ell$, where the initial and boundary data are prescribed as follows

$$\begin{cases} u_t + uu_x + \epsilon^2 u_{xxx} &= 0, & x \in [-\ell, \ell], t > 0, \\ u(x, 0) &= 3(1 - \tanh((x - x_0)/w) - 2), \\ u(-\ell, t) &= 3(1 - \tanh((-\ell - x_0)/w) - 2), \\ u(\ell, t) &= 3(1 - \tanh((\ell - x_0)/w) - 2), \\ u_x(\ell, t) &= 0. \end{cases} \quad (37)$$

For example, if $w = 1$ and $\ell - x_0 = 20$, we have $u(-\ell, t) \approx 0$ and $u(\ell, t) \approx -6$. The existence and uniqueness of solution of the above IBVP is discussed in [8].

The numerical scheme we adopt for solving Eq. (37) is a non-oscillatory explicit finite-difference method [31]. The spatial and temporal discretization for the algorithm is

$$\begin{aligned} \frac{1}{2} \left(\frac{u_{j-1}^{n+1} - u_{j-1}^n}{\Delta t} + \frac{u_{j+1}^n - u_{j+1}^{n-1}}{\Delta t} \right) &= - \left(\frac{u_{j+1}^n + u_j^n + u_{j-1}^n}{3} \right) \frac{u_{j+1}^n - u_{j-1}^n}{\Delta x} \\ &\quad - \frac{\epsilon^2}{2\Delta x^3} (u_{j+2}^n - 2u_{j+1}^n + 2u_{j-1}^n - u_{j-2}^n). \end{aligned} \quad (38)$$

Applying the von Neumann analysis for the above scheme yields the stable condition for the scheme

$$\frac{\Delta t}{\Delta x} < \frac{2}{\max_{x,t} |u| + 4\epsilon^2/\Delta x}. \quad (39)$$

Using the same scaling variables as Eq. (3) and Eq. (4), the scaled KdV equation is

$$u_t + L^{-\alpha-\beta+1}uu_x + \epsilon^2 L^{-3\beta+1}u_{xxx} = 0. \quad (40)$$

Here we drop the subscript L for u and $\tilde{\cdot}$ for t and x . Since the amplitude of DSWs saturates at $6c^2$, it is not necessary to scale the amplitude and hence we set $\alpha = 0$ for our numerical RG calculations. Also, similar to the Burgers equation, we choose to retain the coefficient of the dispersion term unscaled. This results in $\beta = 1/3$ at all time for our numerical RG calculations, which suggests that the DSW region expands in the order $O(t^{1/3})$ for the RG calculations. We choose $c^2 = 1$. With this set of parameters, Figure 5 and Figure 6 are the comparisons between direct numerical simulations and numerical RG calculations. The initial condition is a single-step tangent profile. The graphs show that the numerical RG procedure accurately capture the DSWs in a confined domain and the results are consistent with that in the literature [2, 3]. Moreover a simple calculation below will illustrate that the numerical RG procedure is more efficient than direct numerical calculation. Suppose that the final time for a

direct simulation is $t = L^n$ and the number of solitons in the region of DSWs at the final time is N_s . Assume that the spacial grid-size required to resolve these solitons is Δx . For this Δx , the required temporal step-size is $\Delta t = O((\Delta x)^2)$, by the stable condition (39). Therefore the total number of time steps required for the simulation is $L^n/\Delta t \sim L^n/(\Delta x)^2$. Now for the numerical RG procedure, $t = L^n$ means the number of iterations is n . Since the dispersion coefficient is kept the same, the number of solitons after n iterations is also N_s for the numerical RG procedure. However, because of the spacial scaling, the spacial grid-size required for resolving the solitons is now $\Delta \tilde{x} = L^{-n\beta} \Delta x$. Hence the temporal step-size for stability requirement is $\Delta \tilde{t} = O((\Delta \tilde{x})^2)$. The number of time steps for the numerical RG procedure to the final time is $n(L-1)/\Delta \tilde{t} \sim n(L-1)L^{2n\beta}/(\Delta x)^2$. Since $\beta = 1/3$, the numerator of the above equation is $n(L-1)L^{2n/3}$ and this is less than L^n for large n . Our numerical experiments also confirm that direct numerical simulation is much more time consuming than the numerical RG calculation for long-time simulations. We further remark that if an implicit algorithm is used, for which Δt could be chosen at the same order of Δx [30], then the numerical RG procedure is even more preferable than direct numerical simulation.

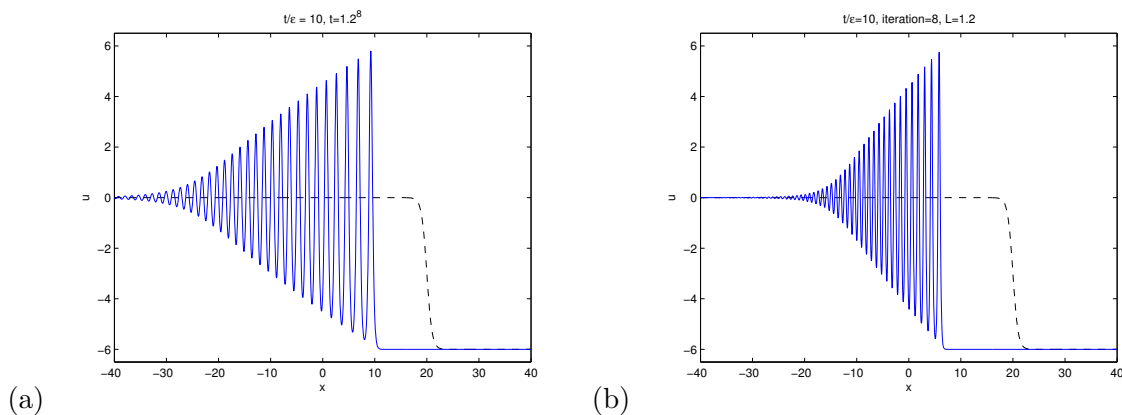


FIGURE 5. (a) Direct numerical simulation. $t/\epsilon = 10$, where $t = 1.2^8$. The spacial and temporal step sizes are $\Delta x = 40/2000$ and $\Delta t = 1.2^8/80000$, respectively. $x_0 = 20$ and $w = 1$. (b) Numerical renormalization group calculation. $\beta = 1/3$, $\alpha = 0$, $L = 1.2$, and $t/\epsilon = 10$. Eight iterations is performed ($n = 8$, i.e. $t = 1.2^8$). For both (a) and (b), dashed line is the initial condition.

4. CUBIC AUTOCATALYTIC CHEMICAL REACTION SYSTEM

The numerical RG procedure described in Section 2.2 assumes that the asymptotic solutions decay or expand at a rate obeying the power law. However, there are differential equations (or systems of differential equations) whose solutions decay at a rate other than the power law, such as the logarithmic decay. For these solutions, the aforementioned procedure is not sufficient to capture the correct decay at the asymptotic region. Nevertheless, the procedure could provide sufficient information that allows us to modify the current algorithm to capture the similarity solutions of those equations.

To illustrate the modification, we consider the Cauchy problem of the chemical reaction system

$$\begin{aligned}
 u_t &= u_{xx} - u^p v^q, \\
 v_t &= dv_{xx} + u^p v^q,
 \end{aligned} \tag{41}$$

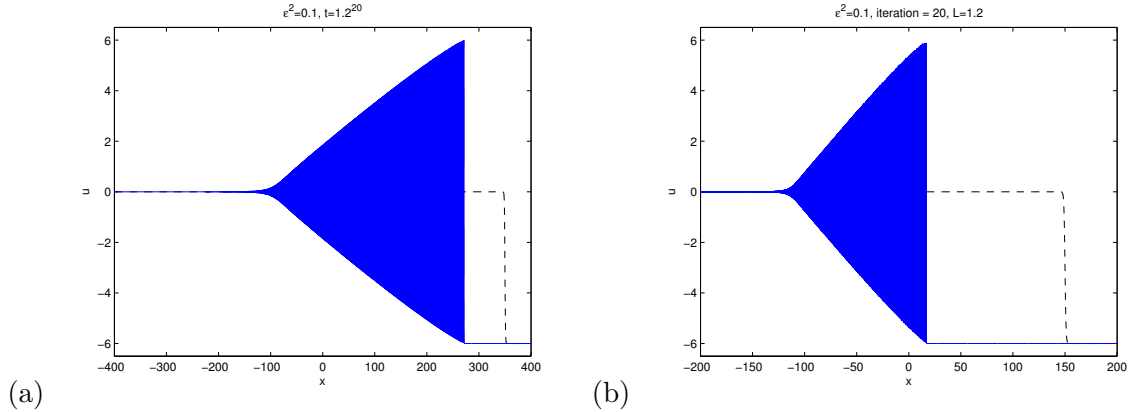


FIGURE 6. (a) Direct numerical simulation. $x_0 = 350$, $w = 1$, $\Delta x = 1/80$, $\Delta t = (1.2)^{20}/32000000 \approx 1.19805 \times 10^{-6}$. $\epsilon^2 = 0.1$. (b) Numerical renormalization group calculation. $\beta = 1/3$, $\alpha = 0$, $L = 1.2$, and $\epsilon^2 = 0.1$. Twenty iterations is performed ($n = 20$, i.e. $t = 1.2^{20}$), $x_0 = 150$, $w = 1$, $\Delta x = 1/80$, and $\Delta t = 1 \times 10^{-6}$. For both (a) and (b), the dashed line is the initial condition.

where $p + q = 3$, $1 \leq p, q \leq 2$, and $d > 0$. This system arises as a model for cubic autocatalytic chemical reactions of the type



with isothermal reaction rate proportional to $u^p v^q$, where u is the concentration of reactant K_1 and v is the concentration of auto-catalyst K_2 [25]. The system is subject to the initial data $u(x, 0) = a_1(x)$ and $v(x, 0) = a_2(x)$, where $a_1, a_2 \geq 0$ and $a_1, a_2 \in L^1(\mathbb{R}) \cap L^\infty(\mathbb{R})$. The above system has been applied for modeling thermal-diffusive combustion problems [11] or mathematical biology [17].

The similarity solutions of this system, based on different values of p and q , are investigated in the papers by Bricmont et al. [11] and Li and Qi [25]. For $p = 1$, $q = 2$, Bricmont et al. show that

$$\begin{aligned} t^{1/2+E_A} u(\sqrt{tx}, t) &\longrightarrow B\psi_A(x), \\ t^{1/2} v(\sqrt{tx}, t) &\longrightarrow A\phi_d(x), \end{aligned} \quad (43)$$

as $t \rightarrow \infty$. Here the total mass $A = \int_{\mathbb{R}} (a_1(x) + a_2(x)) dx$ is conserved along time. B depends continuously on (a_1, a_2) , and the extra decay power E_A in time is due to the critical cubic nonlinearity of the system [11]. ϕ_d is the Gaussian

$$\phi_d(x) = \frac{1}{\sqrt{4\pi d}} e^{-x^2/4d}. \quad (44)$$

Li and Qi extend the above result by considering the values $1 < p, q < 2$ and $p + q = 3$. The nontrivial initial data $a_i \geq 0$, for $i = 1, 2$ are the same as before, whereas the total mass A defined as before is positive. Li and Qi show that

$$\begin{aligned} \sqrt{t}(\log t)^{1/(p-1)} u(\sqrt{tx}, t) &\longrightarrow B\phi_1(x), \\ \sqrt{t}v(\sqrt{tx}, t) &\longrightarrow A\phi_d(x), \end{aligned} \quad (45)$$

as $t \rightarrow \infty$, where

$$B = \left(\frac{4\pi d^{q/2} (p + q/d)^{1/2}}{(p-1)A^q} \right)^{1/(p-1)}, \quad (46)$$

and ϕ_1 is $d = 1$ in Eq. (44). The peculiar phenomena of the similarity solution (45) is that the u -component contains two decays, the regular power-law decay and a logarithmic decay. We illustrate below that the numerical RG algorithm described in section 2.2 is not sufficient to capture the second decay. However, the procedure will provide a clue for the existence of the second decay, and allows us to design a numerical RG procedure to capture the similarity solutions in Eq. (45). We start with the regular numerical RG procedure stated in Section 2.2, i.e. the scaling for t and x is the same as that in Eq. (3), which results in u and v being scaled by

$$\begin{aligned} u_L(\tilde{x}, \tilde{t}) &= L^{\alpha_1} u(x, t) = L^{\alpha_1} u(L^{\beta_1} \tilde{x}, L\tilde{t}), \\ v_L(\tilde{x}, \tilde{t}) &= L^{\alpha_2} v(x, t) = L^{\alpha_2} v(L^{\beta_2} \tilde{x}, L\tilde{t}). \end{aligned} \quad (47)$$

Thus the scalings result in a system of PDEs (dropping the subscript L and $\tilde{}$)

$$\begin{aligned} u_t &= L^{-2\beta_1+1} u_{xx} - L^{-p\alpha_1-q\alpha_2+\alpha_1+1} u^p v^q, \\ v_t &= L^{-2\beta_2+1} v_{xx} + L^{-p\alpha_1-q\alpha_2+\alpha_2+1} u^p v^q. \end{aligned} \quad (48)$$

Similar to the Burgers equation, we choose to keep the diffusion coefficients invariant. Thus $\beta_1 = \beta_2 = 1/2$ at all time, whereas α_1 and α_2 are computed by step (2) in the numerical RG algorithm described in Section 2.2, respectively. With this choice of β_1 and β_2 , the scaled PDE at the n^{th} iteration is

$$\begin{aligned} (u_n) &= (u_n)_{xx} - L^n (L^{-n\bar{\alpha}_{1,n}})^{p-1} (L^{-n\bar{\alpha}_{2,n}})^q (u_n)^p (v_n)^q, \\ (v_n) &= d(v_n)_{xx} + L^n (L^{-n\bar{\alpha}_{1,n}})^p (L^{-n\bar{\alpha}_{2,n}})^{q-1} (u_n)^p (v_n)^q, \end{aligned} \quad (49)$$

where $\bar{\alpha}_{1,n}$ and $\bar{\alpha}_{2,n}$ are defined as $\bar{\alpha}_n$ in Section 2.1. At this stage, we assume that the power-law scaling, based on the hypothesis, is

$$\begin{aligned} u(x, L^n) &\sim \frac{A_u}{L^{n/2}} \phi_u\left(\frac{x}{L^{n/2}}\right), \\ v(x, L^n) &\sim \frac{A_v}{L^{n/2}} \phi_v\left(\frac{x}{L^{n/2}}\right), \end{aligned} \quad (50)$$

where A_u and A_v are constant. The numerical RG iteration, based on the power-law decay assumption, in principle will show $A_{u,n} = L^{n(\alpha_{1,n} - \bar{\alpha}_{1,n})} \sim A_u$, and $A_{v,n} = L^{n(\alpha_{2,n} - \bar{\alpha}_{2,n})} \sim A_v$ (cf. Eq. (18)), as $n \rightarrow \infty$. Unfortunately (or fortunately), this is not the case. The numerical experiment, in fact, shows that $A_{u,n} \rightarrow 0$, while $A_{v,n} \neq 0$ and converges to some constant proportional to the total mass A_{total} , as $n \rightarrow \infty$. Based on this result, we conjecture that the v -component follows the power-law decay, similar to the Burgers equation, while the u -component exists a hidden decay that is not captured by solely assuming the power-law decay.

4.1. A numerical experiment. We conduct a numerical RG experiment using the power-law scaling, Eq. (50), for the above chemical reaction problem with the parameters, $p = q = 1.5$, $d = 0.75$, and $L = 1.2$. The initial data are

$$u(x, 0) = v(x, 0) = \chi_{[-\ell, \ell]}(x) = \begin{cases} 1, & -\ell \leq x \leq \ell, \\ 0, & \text{else.} \end{cases} \quad (51)$$

We choose $\ell = 0.5$ and the computational domain to be $[-10, 10]$. For these initial data, the total conserved mass is $A = 2$. Figure 7(a) is a plot for $\alpha_{1,n}$ and $\alpha_{2,n}$ versus n . From the figure, we expect that $\alpha_{1,n}$ and $\alpha_{2,n}$ both converge to $1/2$ as $n \rightarrow \infty$, although the figure suggests that $\alpha_{1,n}$ may converge much slower than $\alpha_{2,n}$. Since $\beta_n = 1/2$ for all n , from Eq. (18), the convergences of $\alpha_{1,n}$ and $\alpha_{2,n}$, leads to Eq. (50). Moreover, Figure 7(b) are the computed

$A_{u,n}$ and $A_{v,n}$. As expected, $A_{u,n}$ (the dashed-line) approaches to 0 as $n \rightarrow \infty$, while $A_{v,n}$ approaches to a constant A_v . Note that from Eqs. (45) and (50), for $t = L^n$, we have

$$A_{v,n}\phi_v \rightarrow A_v\phi_v = A\phi_d. \quad (52)$$

Since $\phi_v = \sqrt{4\pi d}\phi_d$, $\sqrt{4\pi d}A_v = A$, or $A_v = \frac{1}{\sqrt{4\pi d}}A$. For $d = 0.75$, $A = 2$, $A_v \approx 0.6515$. i.e. $A_{v,n} \rightarrow A_v \approx 0.6515$, and this is exactly what we observe in Figure 7(b).

Figure 8 shows the comparison between the computed Gaussian similarity profile and the predicted theoretical profile in [25] at $n = 3000$, after adjusting the amplitudes. Both components correctly match the prediction, even though the hidden logarithmic decay in u is not captured by the numerical RG algorithm.

Now let's turn our attention to $A_{u,n}$. The fact that $A_{u,n} \rightarrow 0$ as $n \rightarrow \infty$ indicates that there was a "hidden" decay factor that was not captured by the current numerical RG procedure. Taking a log-log plot for $A_{u,n}$ and n , Figure 9 shows that $\log A_{u,n} = (-2)(\log n) + \log C$, as $n \rightarrow \infty$. If we suppose that the hidden decay factor is related to $\log t$, then we could choose C to be $C = A(\log L)^{-2}$. This results in $A_{u,n} = A(\log L^n)^{-2}$, and thus Eq. (50) becomes

$$\begin{aligned} u(x, L^n) &\sim \frac{A^*}{L^{n/2}(\log L^n)^2} \phi_u\left(\frac{x}{L^{n/2}}\right), \\ v(x, L^n) &\sim \frac{A_v}{L^{n/2}} \phi_v\left(\frac{x}{L^{n/2}}\right). \end{aligned} \quad (53)$$

Eq. (53) is evidently the similarity (asymptotic) solutions of the system of chemical-reaction equations for $t = L^n$ and $p = q = 3/2$ (cf. Eq. (45)).

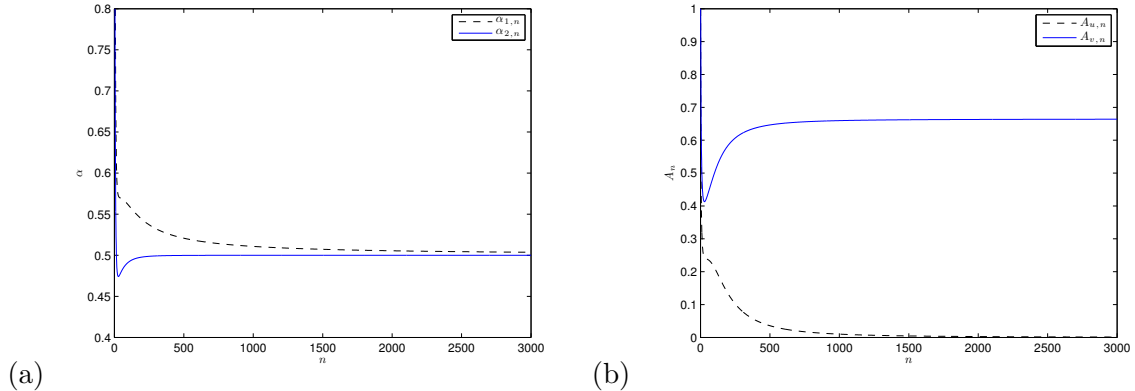


FIGURE 7. Computed scaling factors by the numerical RG procedure stated in Section 2.2 for the chemical reaction system. (a) $\alpha_{1,n}$ and $\alpha_{2,n}$ (b) $A_{u,n}$ and $A_{v,n}$.

5. MODIFIED RG ALGORITHM FOR LOGARITHMIC DECAY

The above experiment suggests that the component v has the decay factor \sqrt{t} , but the component u may have more than one decay factor. Without the asymptotic formula (45), in principle, we do not know what the decay factors are. However, if we "guess" that one of them is also \sqrt{t} based on Figures 7 and 9, and suppose that the other is related to $\log t$ with some unknown power γ , then the solution in the asymptotic region gives us an idea how to compute the power γ_n at the end of each iteration. Taking the hint from Eq. (45), at times t and Lt ,

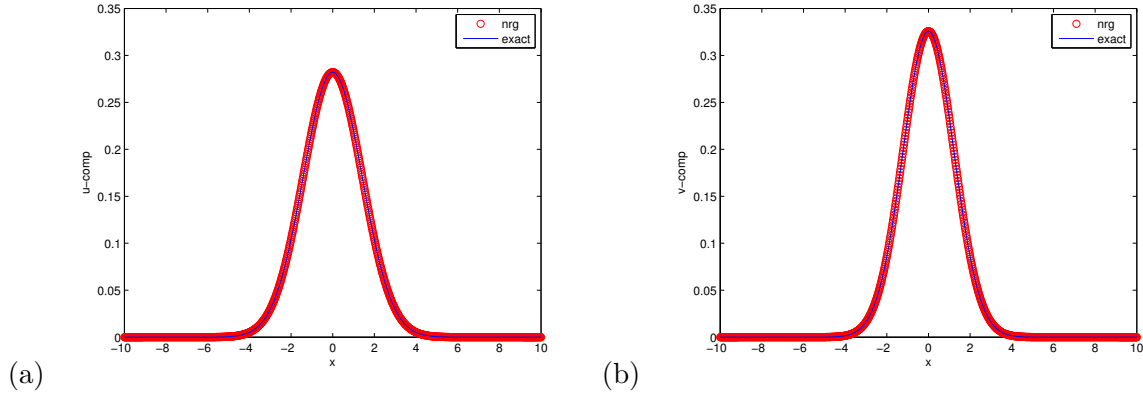


FIGURE 8. Comparison between the computed Gaussian similarity profile by Algorithm 1 and the predicted theoretical profile in [25] at $n = 3000$, after adjusting the amplitudes. (a) u -component, (b) v -component.

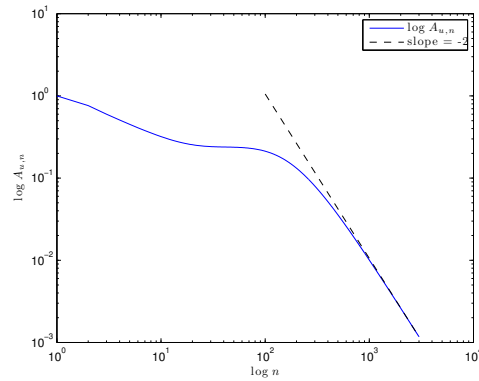


FIGURE 9. log–log plot for $A_{u,n}$ and n . The dashed-line is the straight line whose slope is equal to -2 .

the ratio of the solutions is

$$\frac{\|u(x, t)\|_\infty}{\|u(x, Lt)\|_\infty} = \frac{L^{1/2} t^{1/2} (\log Lt)^\gamma}{t^{1/2} (\log t)^\gamma} = L^{1/2} \left(\frac{(\log Lt)}{(\log t)} \right)^\gamma \quad (54)$$

To modify the numerical RG procedure for this case, we observe that at the end of the $(n-1)^{th}$ iteration $t = L^{n-1}$,

$$L^{1/2} \left(\frac{\log L^n}{\log L^{n-1}} \right)^{\gamma_n} = L^{1/2} \left(\frac{n}{n-1} \right)^{\gamma_n} = \frac{\|u_{n-1}(\cdot, 1)\|_\infty}{\|u_{n-1}(\cdot, L)\|_\infty}, \quad n > 1, \quad (55)$$

following Eq. (54). Note that for the case $n = 1$, γ_1 is computed by the power-law scaling,

$$L^{\gamma_1} = \frac{\|u_0(\cdot, 1)\|_\infty}{\|u_0(\cdot, L)\|_\infty}. \quad (56)$$

Eqs. (55) and (56) suggest that for the u -component, the initial condition for the next iteration is set by

$$u_n(x, 1) = L^{1/2} \left(\frac{n}{n-1} \right)^{\gamma_n} u_{n-1}(L^{1/2}x, L), \quad \text{for } n > 1, \quad (57)$$

and

$$u_1(x, 1) = L^{\gamma_1} u(L^{1/2}x, L), \quad \text{for } n = 1. \quad (58)$$

Here we have chosen $\beta_1 = \beta_2 = 1/2$ in order to keep the diffusion coefficients unchanged. Note that from Eq. (57), at the end of the n^{th} iteration ($n > 1$), the iterative solutions u_n and v_n are related to the solutions of the PDE's by

$$\begin{aligned} u_n(x, t) &= L^{\gamma_1 + (n-1)/2} \prod_{k=2}^n \left(\frac{k}{k-1} \right)^{\gamma_k} u(L^{n/2}x, L^n t), \\ v_n(x, t) &= L^{n\bar{\alpha}_{2,n}} v(L^{n/2}x, L^n t), \end{aligned} \quad (59)$$

where $\bar{\alpha}_{2,n} = (\alpha_{2,1} + \dots + \alpha_{2,n})/n$. Eq. (59) implies that

$$\begin{aligned} u(x, t) &= L^{-\gamma_1 - (n-1)/2} \prod_{k=2}^n \left(\frac{k-1}{k} \right)^{\gamma_k} u_n(L^{-n/2}x, L^{-n}t), \\ v(x, t) &= L^{-n\bar{\alpha}_{2,n}} v_n(L^{-n/2}x, L^{-n}t). \end{aligned} \quad (60)$$

Hence for the n^{th} iteration ($n \geq 1$), the scaled system of PDEs for u_n and v_n is

$$\begin{aligned} (u_n)_t &= (u_n)_{xx} - L^n L^{(-p+1)\gamma_1} (L^{-(n-1)/2})^{(p-1)} \left(\prod_{k=2}^n \left(\frac{k-1}{k} \right)^{\gamma_k} \right)^{p-1} (L^{-n\bar{\alpha}_{2,n}})^q (u_n)^p (v_n)^q, \\ (v_n)_t &= d(v_n)_{xx} + L^n L^{-p\gamma_1} (L^{-(n-1)/2})^p \left(\prod_{k=2}^n \left(\frac{k-1}{k} \right)^{\gamma_k} \right)^p (L^{-n\bar{\alpha}_{2,n}})^{q-1} (u_n)^p (v_n)^q, \end{aligned} \quad (61)$$

for $\beta_1 = \beta_2 = 1/2$. For $n = 0$, the unscaled equation (41) is solved.

Now, similar to the steps from Eq. (13) to Eq. (18), we can define a variable $A_{u,n}$ for the u -component, so that we can monitor $A_{u,n}$ for convergence. From the first equation in Eq. (53) and the first equation in Eq. (59), we have

$$\begin{aligned} u(L^{n/2}x, L^n) &\sim L^{-n/2} (\log L^n)^{-\gamma} A\phi(x), \\ u_n(x, 1) &= L^{\gamma_1 + (n-1)/2} \prod_{k=2}^n \left(\frac{k}{k-1} \right)^{\gamma_k} u(L^{n/2}x, L^n). \end{aligned} \quad (62)$$

If we let $A_* = A(\log L)^{-\gamma}$ and assume that $\gamma_n \rightarrow \gamma$ as $n \rightarrow \infty$, Eq. (62) implies

$$\begin{aligned} u_n(x, 1) &\sim L^{\gamma_1 + (n-1)/2} \prod_{k=2}^n \left(\frac{k}{k-1} \right)^{\gamma_k} L^{-n/2} n^{-\gamma_n} A_* \phi(x) \\ &\sim L^{\gamma_1 - 1/2} \prod_{k=2}^n \left(\frac{k}{k-1} \right)^{\gamma_k - \gamma_n} A_* \phi(x), \end{aligned} \quad (63)$$

The above equation holds, since $\gamma_n \rightarrow \gamma$ for $n \rightarrow \infty$ and thus $n^{-\gamma_n} = \prod_{k=2}^n \left(\frac{k}{k-1} \right)^{-\gamma_n}$ for $n \rightarrow \infty$. Eq. (63) is equivalent to

$$L^{1/2 - \gamma_1} \prod_{k=2}^n \left(\frac{k}{k-1} \right)^{\gamma_n - \gamma_k} u_n(x, 1) \sim A_* \phi(x). \quad (64)$$

If we define

$$A_{u,n} = L^{1/2 - \gamma_1} \prod_{k=2}^n \left(\frac{k}{k-1} \right)^{\gamma_n - \gamma_k}, \quad n > 1, \quad (65)$$

Algorithm 2 Numerical RG procedure for the chemical reaction system

for $n = 0, 1, 2, \dots$, until convergence **do**

1. Start with the IVP (41) for $n = 0$. Evolve u_n and v_n from $t = 1$ to $t = L$, using the IVP (61) for $n \geq 1$.
2. Compute γ_n for the u -component by

$$L^{\gamma_1} = \frac{\|u_0(\cdot, 1)\|_\infty}{\|u_0(\cdot, L)\|_\infty},$$

$$L^{1/2} \left(\frac{n}{n-1} \right)^{\gamma_n} = \frac{\|u_{n-1}(\cdot, 1)\|_\infty}{\|u_{n-1}(\cdot, L)\|_\infty}, \quad n \geq 2. \quad (67)$$

Compute $\alpha_{2,n}$ for the v -component by

$$L^{\alpha_{2,n}} = \frac{\|v_{n-1}(\cdot, 1)\|_\infty}{\|v_{n-1}(\cdot, L)\|_\infty}.$$

3. Compute $A_{u,n} = L^{1/2-\gamma_1} \prod_{k=2}^n \left(\frac{k}{k-1} \right)^{\gamma_n - \gamma_k}$, $n > 1$; $A_{v,n} = L^{n(\alpha_{2,n} - \bar{\alpha}_{2,n})}$, where $\bar{\alpha}_{2,n} = (\alpha_{2,1} + \dots + \alpha_{2,n})/n$.
4. Set initial data for the next iteration by $f_{u,n+1} = L^{1/2} \left(\frac{n}{n-1} \right)^{\gamma_n} u_n(L^{1/2}x, L)$ and $f_{v,n+1}(x) = L^{\alpha_{2,n}} v_n(L^{1/2}x, L)$.

end for

we expect that $A_{u,n} \rightarrow A_*$ for n large enough, provided $u_n(x, 1) \rightarrow \phi(x)$. Since $\phi = \sqrt{4\pi}\phi_1$, where ϕ_1 is the Gaussian function in Eq. (44) with $d = 1$, this implies that $A\sqrt{4\pi} = B$, where B is the theoretical prediction in Eq. (46). Therefore

$$A_{u,n} \rightarrow A_* = A(\log L)^{-\gamma} = \frac{B(\log L)^{-\gamma}}{\sqrt{4\pi}}. \quad (66)$$

For $A_{v,n}$ we expect $A_{v,n} \rightarrow A_v = \frac{A}{\sqrt{4\pi}}$, where A is the conserved total mass, the same as before.

We summarize the modified numerical RG procedure for the chemical reaction problem with the choice of parameters $\beta_1 = \beta_2 = 1/2$ in Algorithm 2.

6. A NUMERICAL EXPERIMENT FOR THE LOGARITHMIC DECAY

To illustrate that the modified RG algorithm accurately captures the hidden logarithmic decay, we apply Algorithm 2 to the diffusion-reaction equations Eq. (41) with $p = q = 3/2$. For this set of parameters, the asymptotical behavior of the solutions follows Eqs. (45) and (46). Thanks to the choice of $\beta_1 = \beta_2 = 1/2$, the diffusivities in Eq. (61) are kept to be 1 and d , respectively. Here we choose $d = 3/4$. The system of PDEs (61) is discretized by an explicit second-order method (forward Euler for the time derivative and the second-order center difference for the spatial second derivative). The parameters used in our numerical RG algorithm are $L = 1.25$, $x \in [-10, 10]$, $dx = 0.04$, and $dt = 0.00025$. The number of iterations for numerical RG is 3000. The theoretical prediction for the critical exponents is $\gamma = 2$ (power of the logarithmic decay for u) and $\alpha = 0.5$ (power of the power law decay for v). Figure 10 shows that Algorithm 2 accurately captures these two exponents. At the mean time, the theoretical prediction for the pre-factor A_* is $A_* \approx 1016.89$, computed by Eq. (66), and the pre-factor A_v is $A_v \approx 0.6515$, the same as our previous calculation, and we observe from Figure 11 that both $A_{u,n}$ and $A_{v,n}$ numerically converges to their theoretical values, respectively.

Finally, in the the previous section 4.1, our calculation suggests that the original numerical RG algorithm captures the power law exponents and produces the final similarity profiles that

match the theoretical prediction in [25] without taking into account the logarithmic decay. In this experiment, we use the hint from the previous calculation to assume the exponent of the power law decay for the u component. We modified the RG algorithm to include the logarithmic decay. The modified RG algorithm captures the critical exponents and render the numerically convergent pre-factors for both components. It remains to show whether the similarity profiles produced by the modified RG algorithm match the theoretical prediction. Sure enough, Figure 12 shows that the modified RG algorithm produces the similarity profiles that match the theoretical prediction exactly after we adjust the amplitudes by multiplying the factor $1/\sqrt{4\pi d}$, where $d = 1$ for u and $d = 3/4$ for v , respectively.

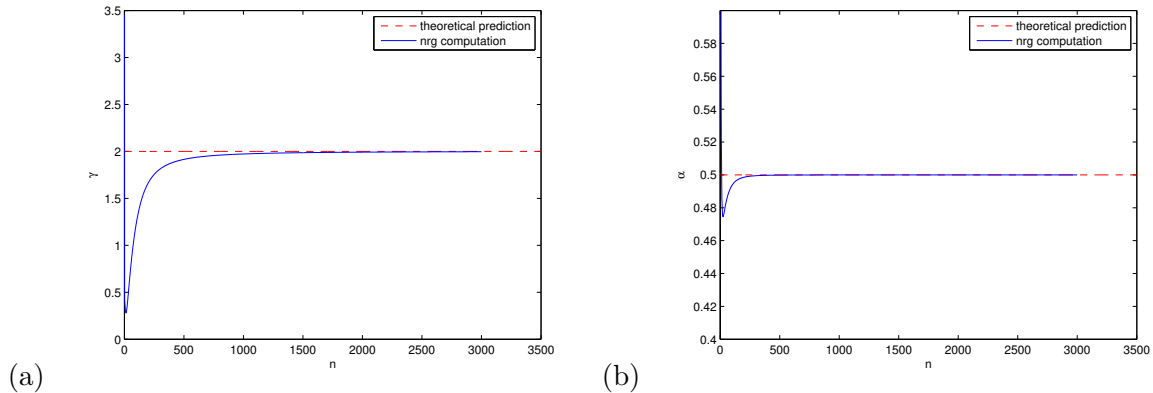


FIGURE 10. Comparison of the theoretical prediction and numerical RG computation for the exponents: (a) the sequence of logarithmic decay exponent $\gamma_n \rightarrow \gamma = 2$ for u , and (b) the sequence of the power law decay exponent $\alpha_n \rightarrow \alpha = 0.5$ for v .

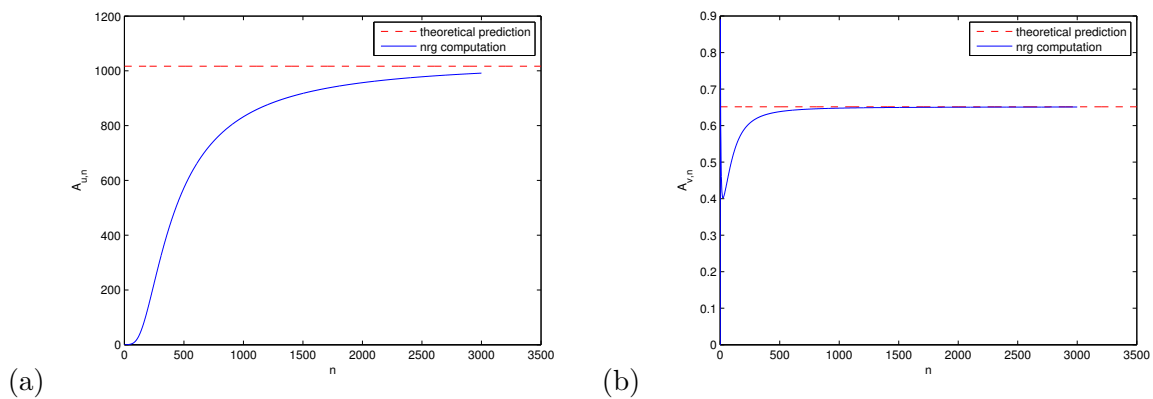


FIGURE 11. Comparison of the theoretical prediction and numerical RG computation for the pre factors: (a) $A_{u,n} \rightarrow A_* \approx 1016.89$, and (b) $A_{v,n} \rightarrow A_v \approx 0.6515$.

7. CONCLUDING REMARKS

We have presented and systematically examined a numerical procedure, based on the RG theory for PDEs, that renders the detailed and efficient computation of asymptotically self-similar dynamics in solutions of PDEs. The effectiveness and robustness of the proposed

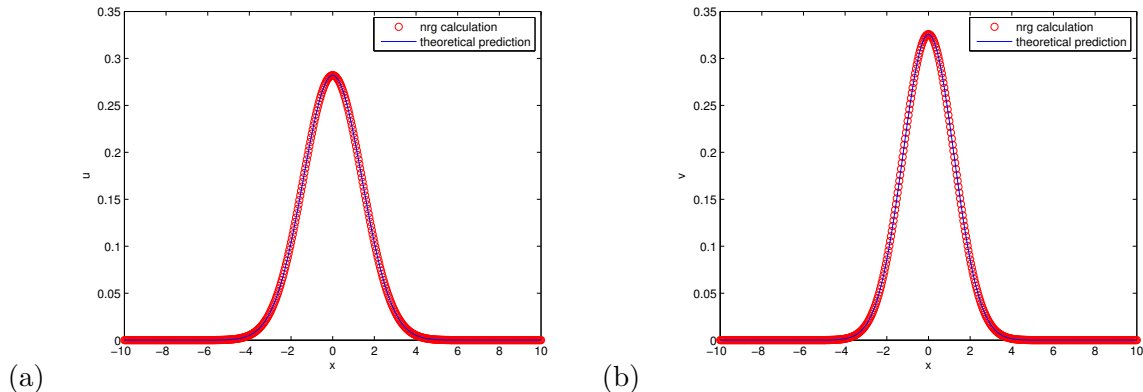


FIGURE 12. Comparison between the computed Gaussian similarity profile by Algorithm 2 and the predicted theoretical profile in [25] at $n = 3000$, after adjusting the amplitudes. (a) u -component, (b) v -component.

algorithms were illustrated through several examples of quasilinear and nonlinear PDEs combining diffusive, reactive and nonlinear propagation effects. It is worth noting that the modified RG algorithm presented in Sections 5 and 6 for the nonlinear system of cubic autocatalytic chemical reaction equations nicely responds to the remark made by Li and Qi [25]:

“The appearance of $\log t$ indicates the analysis is more involved and subtle. In particular, it is well known in the scientific computation field that a scaling of $\log t$ is hardly detectable in computation.”

by detecting the extra decay and capturing the power of logarithmic decay.

We refer readers to [23] for some preliminary results of the calculations of multidimensional problems by using the similar numerical scaling strategy described in this paper. A proper modification of the described RG algorithm can be used to compute traveling waves and is currently under our investigation. We are also investigating the applicability of an adapted version of the RG algorithm to blow-up problems. We expect to report our results in the near future.

8. ACKNOWLEDGEMENT

GAB thanks the Department of Mathematics at the University of Wyoming for the hospitality which made possible this collaboration. FCF thanks Nigel Goldenfeld and Yoshitsugu Oono for their insightful discussion on the renormalization group method.

REFERENCES

- [1] Ablowitz, M. J., Baldwin, D. E., and Hoefer, M. A.. Soliton generation and phases in dispersive shock and rarefaction wave interaction, *Phy. Rev. E*, **80**, 016603, 2009.
- [2] Ablowitz, M. J. and Baldwin, D. E.. Interactions and asymptotics of dispersive shock waves - Korteweg-de Vries equation, *Phys. Lett. A*, **377**, 555-559, 2013.
- [3] Ablowitz, M. J. and Baldwin, D. E.. Dispersive shock wave interactions and asymptotics, *Phys. Rev. E*, **87**, 022906, 2013.
- [4] Angenent, S. B., Aronson, D. G., Betelú, S. I., and Lowengrub, J. S.. Focusing of an elongated hole in porous medium flow, *Phys. D*, **151**, 228–252, 2001.
- [5] Berger, M. and Kohn, R.. A rescaling algorithm for the numerical calculation of blowing-up solutions, *Comm. Pure Appl. Math.*, **XI.I**, 841–863, 1988.
- [6] Betelú, S. I., Aronson, D. G., and Angenent, S. B.. Renormalization study of two-dimensional convergent solutions of the porous medium equation, *Phys. D*, **138**, 344–359, 2000.

- [7] Bona, J. Promislow, K., and Wayne, G.. On the asymptotic behavior of solutions to nonlinear, dispersive, dissipative wave equations, *Mathematics and Computers in Simulation*, **37**, 265–277, 1994.
- [8] Bona, J. L., Sun, S. M. and Zhang B.-Y.. A nonhomogeneous boundary-value problem for the Korteweg-de Vries equation posed on a finite domain, *Comm. Partial Diff. Eq.*, **28**, 1391–1436, 2003.
- [9] Braga, G. A., Furtado, F., Moreira, J. M, and Rolla, L. T. .. Renormalization group analysis of nonlinear diffusion equations with periodic coefficients, *SIAM MMS*, **1**(4), 630–644, 2003.
- [10] Bricmont, J and Kupiainen, A.. Renormalizing partial differential equations, Constructive Physics, Berlin: Springer, Lecture Notes in Physics, **446**, 83–115, 1995.
- [11] Bricmont, J., Kupiainen, A., and Xin, J.. Global large time self-similarity of a thermal-diffusive combustion system with critical nonlinearity, *J. Diff. Eqns*, **130**, 9–35, 1996.
- [12] Bricmont, J., Kupiainen, A., and Lin, G.. Renormalization group and asymptotics of solutions of nonlinear parabolic equations, *Comm. Pure Appl. Math.*, **47**, 893–992, 1994.
- [13] Caginalp, G.. Renormalization and scaling methods for nonlinear parabolic systems, *Nonlinearity* , **10**, 1217–1229, 1997.
- [14] Caginalp, G.. A renormalization group approach to blow-up and extinction exponents, *Nonlinear Analysis*, **10**, 2187–2202, 2001.
- [15] Chen L., Goldenfeld, N., and Oono, Y.. Renormalization group theory for the modified porous medium equation, *Phys. Rev. A*, **44**, 6544–6550, 1991.
- [16] Chen L., and Goldenfeld, N.. Numerical renormalization group calculations for similarity solutions and traveling waves, *Phys. Rev. E*, **51**, 5577–5581, 1995.
- [17] Feireisl, E., Hilhorst, D., Mimura, M., and Weidenfeld, R.. On some reaction-diffusion systems with nonlinear diffusion arising in biology, *H. Berestycki and Y. Pomeau (eds.), Nonlinear PDE's in Condensed Matter and Reactive Flows*, 115–125, 2002.
- [18] Fibich, G. and Wang, X. P.. Stability of solitary wave for nonlinear Schrödinger equations with inhomogeneous nonlinearities, *Phys. D*, **175**, 96–108, 2003.
- [19] Gell-Mann, M. and Low, F. E.. Quantum electrodynamics at small distances, *Phys. Rev.*, **95**, 1300–1312, 1954.
- [20] Goldenfeld, N. *Lectures on Phase Transitions and the Renormalization Group*, Addison-Wesley, 1992.
- [21] Goldenfeld, N, Martin ,O, Oono, Y., and Liu ,F.. Anomalous dimensions and the renormalization group in a nonlinear diffusion process, *Phys. Rev. Lett.*, **65**, 1361–1364, 1990.
- [22] Goldenfeld, N, Martin ,O, and Oono, Y.. Asymptotics of partial differential equations and the renormalization group, *Phys. Rev. Lett.*, **65**, 1361–1364, 1990.
- [23] Isaia, V.. *Asymptotic Behavior of Nonlinear Parabolic PDEs via a Renormalization Group Approach: a Numerical Study*, Ph.D. thesis, Department of Mathematics, University of Wyoming, 2002.
- [24] LeMesurier, B., Papanicolaou, G., Sulem, C., and Sulem, P.-L.. The focusing singularity of the cubic Schrödinger equation, *Phys. Rev. A*, **34**, 1200–1210, 1986.
- [25] Li, Y. and Qi, Y. W.. The global dynamics of isothermal chemical systems with critical nonlinearity, *Nonlinearity*, **16**, 1057–1074, 2003.
- [26] Merdan, H. and Caginalp, G.. Decay of solutions to nonlinear parabolic equations: renormalization and rigorous results, *DCDS-B*, **3**, 246–273, 2003.
- [27] Promislow, K.. A renormalization method for modulational stability of quasi-steady patterns in dispersive systems, *SIAM J. Math. Anal.*, **33**(6) 1455–1482, 2002.
- [28] Ren, W. and Wang, X. P.. An iterative grid redistribution method for singular problems in multiple dimensions, *J. Comp. Phys.*, **159**, 246–273, 2000.
- [29] San Martin, L. and Oono, Y.. Physics-motivated numerical solvers for partial differential equations, *Phys. Rev. E*, **57**, 4795–4810, 1998.
- [30] Skogestad J. O. and Kalisch, H.. A boundary value problem for the KdV equation: Comparison of finite-difference and Chebyshev methods, *Math. Comp. Simul.*, **80**, 151–163, 2009.
- [31] Wang, H.-P., Wang, Y.-S, Hu, Y.-Y.. An explicit scheme for the KdV equation, *Chin. Phys. Lett.*, **25**(7), 2335–2338, 2008.
- [32] Whitham, G. B.. *Linear and Nonlinear Waves*, JOHN WILEY & SONS, 1974.
- [33] Wilson, K.. Renormalization group and critical phenomena I , *Phys. Rev. B*, **4**, 3174–3183, 1971.
- [34] Wilson, K.. Renormalization group and critical phenomena II , *Phys. Rev. B*, **4**, 3184–3205, 1971.

DEPARTMENT OF MATHEMATICS, FEDERAL UNIVERSITY OF MINAS GERAIS, BRAZIL
E-mail address: gdabraga@gmail.com

DEPARTMENT OF MATHEMATICS, UNIVERSITY OF WYOMING, LARAMIE, WY 82071-3036, USA
E-mail address: furtado@uwyo.edu, TEL:307-766-4321

DEPARTMENT OF MATHEMATICS, UNIVERSITY OF WYOMING, LARAMIE, WY 82071-3036, USA
E-mail address: llee@uwyo.edu, TEL:307-766-4368